METHODS

Protein expression and purification. A synthetic gene comprising the entire BRI1 ectodomain (residues 29-788) and codon optimized for expression in *Trichoplusia ni* was synthesised by Geneart (Regensburg, Germany). The gene was cloned into a modified pBAC-6 transfer vector (Novagen), providing a glycoprotein 64 signal peptide and a C-terminal TEV (tobacco etch virus protease) cleavable Strep-9xHis tandem affinity tag. Recombinant baculoviruses were generated by co-transfecting the transfer vector with linearised baculovirus DNA (ProFold-ER1, AB vector, San Diego, USA) and amplified in Sf9 cells. The fusion protein was expressed in Hi5 cells using a multiplicity of infection of 5, and harvested from the medium 4 days post infection by tangential flow filtration using a 30 kDa MWCO (molecular weight cut-off) filter membrane (GE Healthcare). BRI1 was purified by sequential Co^{2+} (His select gel, Sigma) and Strep (Strep-Tactin Superflow high-capacity, IBA, Göttingen, Germany) affinity chromatography. Next, the tandem affinity tag was removed by incubating purified BRI1 with recombinant TEV protease in 1:100 molar ratio. The cleaved tag and the protease were separated from BRI1 by size exclusion chromatography on a Superdex 200 HR10/30 column (GE Healthcare) equilibrated in 20 mM Hepes pH 7.5, 100 mM NaCl, 1 mM EDTA). Monomeric peak fractions were concentrated to ~15 mg/mL and snap frozen in liquid nitrogen. About 50 – 80 μg of purified BRI1 could be obtained from 1 litre of insect cell culture.

Crystallisation and data collection. Initial crystals of BRI1 appeared in 18% PEG 4,000, 0.8 M KCl using the counter diffusion method. Diffraction quality crystals of about 300x80x600 μm could be grown after multiple rounds of microseeding at room-temperature by vapour diffusion in hanging drops composed of 1.25 μL of protein solution (15 mg/mL) and 1.25 μL of crystallisation buffer (14% PEG 4,000, 0.2 M $(NH_4)_2SO_4$, 0.1 M citric acid pH 4.0) suspended above 1.0 mL of the mother liquor as the reservoir solution. For structure solution crystals were stabilised, derivatised and cryo-protected by serial transfer into 16% PEG 4,000, 1.7 M Na malonate pH (4.0) and 0.5 M NaI, and cryo-cooled in liquid nitrogen. Single-wavelength anomalous diffraction (SAD) data to 2.9 Å resolution were collected on a Rigaku MicroMax rotating anode equipped with a copper filament, osmic mirrors and an R-AXIS IV++ detector. Native crystals were transferred to a cryo-protective solution containing 16 % PEG 4,000 and 1.7 M Na malonate (pH 4.0) and flash-cooled in liquid nitrogen. An isomorphous native dataset to 2.5 Å was collected at beam-line 8.2.1 of the Advanced Light Source (ALS), Berkeley. The hormone-bound structure was obtained by dissolving brassinolide (Chemiclones Inc., Waterloo, Canada) to a concentration of 1 mM in 100% DMSO. This stock solution was diluted to a final concentration of about 50 μM in protein storage buffer (20

mM Hepes pH 7.5, 100 mM NaCl, 1 mM EDTA). Purified BRI1 protein was added to a final concentration of about 12.5 μM (1.5 mg/mL) and the mixture was incubated at room-temperature for 16 h. Next, the complex was re-concentrated to 18 mg/mL, and immediately used for crystallisation. Crystals appeared under similar conditions as established for the unbound form and diffracted again to about 2.5 Å. Data processing and scaling was done with XDS[51] (version: May 2010) (Supplementary Table 1).

Structure Solution and Refinement. The program XPREP (Bruker AXS) was used to scale native and derivative data for SIRAS (single isomorphous replacement with anomalous scattering) analysis. Using data between 30-3.7 Å, SHELXD[52] located 52 iodine sites (CC All/Weak 42.50/19.82). 16 consistent sites were input into the program SHARP[53] for phasing and identification of 10 additional sites at 2.9 Å resolution (Supplementary Fig. 1a). Refined heavy atom sites and phases were input into phenix.resolve[54] for density modification and phase extension to 2.5 Å (final FOM was 0.55). The resulting electron density map was readily interpretable (Supplementary Fig. 1b), and the structure was completed in alternating cycles of model building in COOT[55] and restrained TLS refinement in phenix.refine[56]. Refinement statistics are summarised in Supplementary Table 1. The crystals contain one BRI1 monomer per asymmetric unit with a solvent content of ~60%. The final models comprise residues 29 – 771, with the C-termini (residues 772-788) being completely disordered. The structure contains 25 LRRs as initially proposed[3], and not 24 LRRs as concluded from later modelling studies[13]. Loop residues 590, 637 and 638 in the island domain appear disordered in the unliganded structure. Amino acids whose side-chains could not be modelled with confidence were truncated to alanine (2% of all residues). Analysis with Molprobity[57] suggested that both refined models have excellent stereochemistry, with the free form having 93.3% of all residues in the favoured region of the Ramachandran plot, and no outliers (Molprobity score is 2.2 corresponding to the 90th percentile for structures (N=6,681) at 2.52Å ± 0.25Å resolution). The brassinolide complex structure has 92.7% of all residues in the favoured region of the Ramachandran plot and no outliers (Molprobity score is 2.3 corresponding to the 86th percentile for structures (N=6,632) at 2.54Å ± 0.25Å resolution). Structural visualization was done with POVScript+[58] and POV-Ray (http://www.povray.org).

Size-exclusion chromatography was performed using a Superdex 200 HR 10/30 column (GE Healthcare) pre-equilibrated in 25 mM citric acid / sodium citrate buffer (pH 4.5), 100 mM NaCl. 100 μL of sample (5 mg/mL) was loaded onto the column and elution at 0.6 mL/min was monitored by ultraviolet absorbance at 280 nm. Incubation with brassinolide was performed as described in the crystallisation section.

Homology Modelling of the AtBAK1 ectodomain (residues 27-227; Uniprot http://www.uniprot.org; accession Q94F62) was performed with the program MODELLER[59] using the BRI1 and PGIP structures as template. Structure-based sequence alignments were done using T-COFFEE[60]. BRI1 and BAK1 share ~35% , PGIP and BAK1 share ~31% sequence identity, with the LRR and N-cap consensus sequences being highly conserved.

References

51. Kabsch, W. Automatic processing of rotation diffraction data from crystals of initially unknown symmetry and cell constants. *J. Appl. Crystallogr.* **26**, 795-800 (1993).
52. Sheldrick, G.M. A short history of SHELX. *Acta Crystallogr., A, Found. Crystallogr.* **64**, 112-122 (2008).
53. Bricogne, G., Vonrhein, C., Flensburg, C., Schiltz, M. & Paciorek, W. Generation, representation and flow of phase information in structure determination: recent developments in and around SHARP 2.0. *Acta Crystallogr. D Biol. Crystallogr.* **59**, 2023-2030 (2003).
54. Terwilliger, T.C. et al. Iterative model building, structure refinement and density modification with the PHENIX AutoBuild wizard. *Acta Crystallogr. D Biol. Crystallogr.* **64**, 61-69 (2008).
55. Emsley, P. & Cowtan, K. Coot: model-building tools for molecular graphics. *Acta Crystallogr. D Biol. Crystallogr.* **60**, 2126-2132 (2004).
56. Afonine, P.V., Grosse-Kunstleve, R.W. & Adams, P.D. The Phenix refinement framework. *CCP4 Newsl.* contribution 8 (2005).
57. Davis, I.W. et al. MolProbity: all-atom contacts and structure validation for proteins and nucleic acids. *Nucleic Acids Res.* **35**, W375-383 (2007).
58. Fenn, T.D., Ringe, D. & Petsko, G.A. POVScript+: a program for model and data visualization using persistence of vision ray-tracing. *J. Appl. Crystallogr.* **36**, 944-947 (2003).
59. Sali, A., Potterton, L., Yuan, F., van Vlijmen, H. & Karplus, M. Evaluation of comparative protein modeling by MODELLER. *Proteins* **23**, 318-326 (1995).
60. Notredame, C., Higgins, D.G. & Heringa, J. T-Coffee: A novel method for fast and accurate multiple sequence alignment. *J. Mol. Biol.* **302**, 205-217 (2000).
61. Holm, L., Kääriäinen, S., Rosenström, P. & Schenkel, A. Searching protein structure databases with DaliLite v.3. *Bioinformatics* **24**, 2780-2781 (2008).
62. Kabsch, W. & Sander, C. Dictionary of protein secondary structure: pattern recognition of hydrogen-bonded and geometrical features. *Biopolymers* **22**, 2577-2637 (1983).
63. Belkhadir, Y. et al. Intragenic suppression of a trafficking-defective brassinosteroid receptor mutant in Arabidopsis. *Genetics* **185**, 1283-1296 (2010).

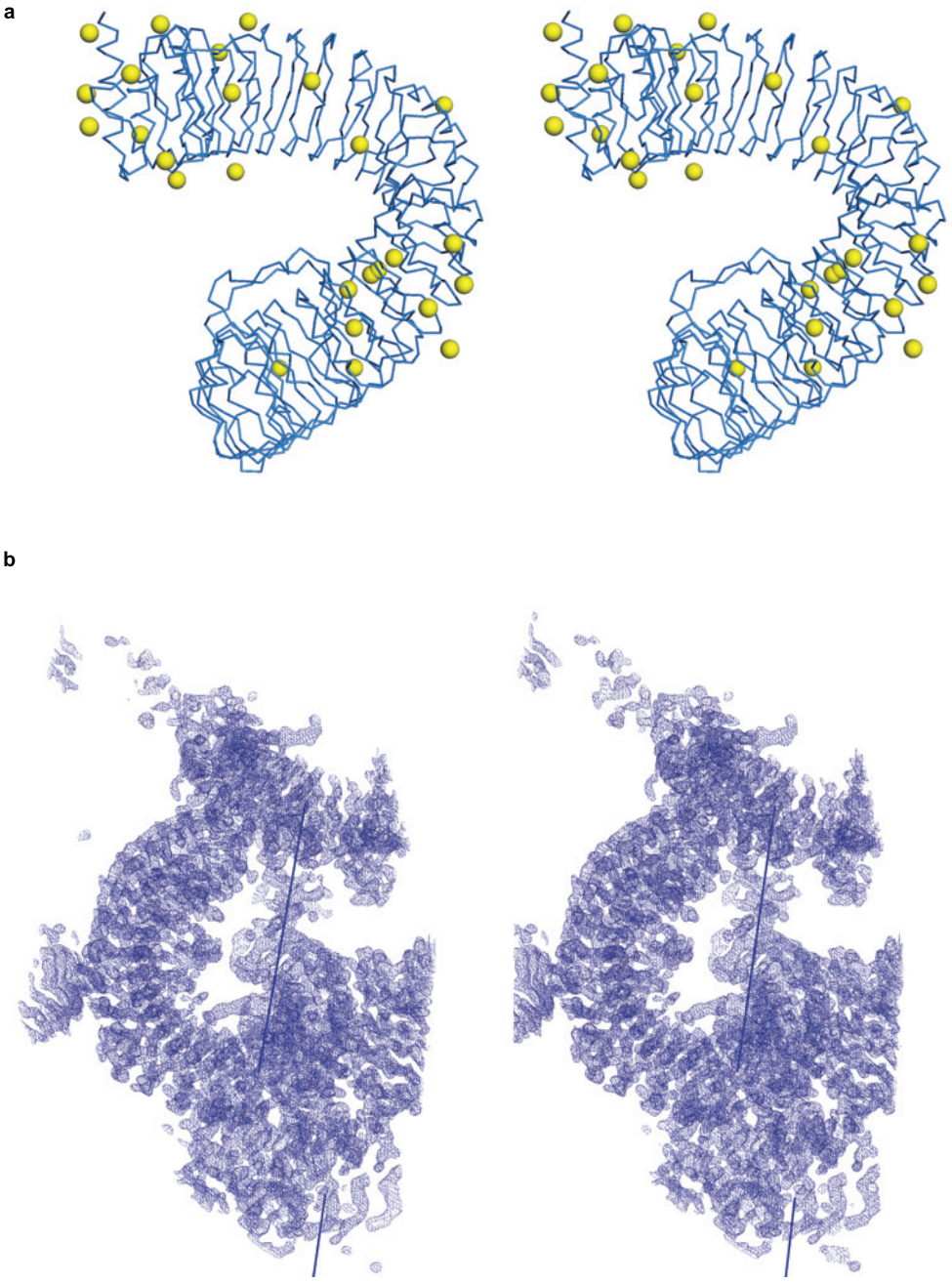

Supplementary Figure 1 | Single Isomorphous Replacement phasing of the BRI1 ectodomain using a sodium iodide shortsoak. a, Stereo view of a C_α trace of the BRI1 structure (in blue) shown together with the 26 heavy atom sites (in yellow) identified with the programs SHELXD[52] and SHARP[53] that were used for SIRAS phasing (min/max/mean refined occupancies are 0.1/0.57/0.33). **b,** Stereo view of the initial $2F_o$-F_c electron density map (contoured at 1.5 σ) obtained after density modification and phase extension to 2.5 Å using the program phenix.resolve[54].

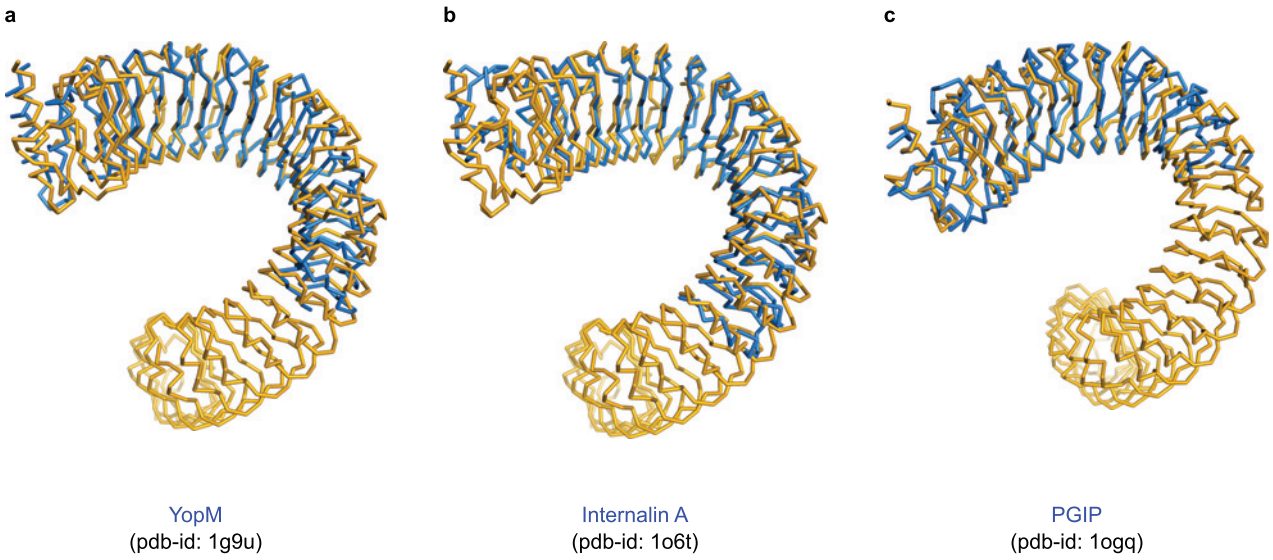

Supplementary Figure 2 | The BRI1 ectodomain is structurally related to bacterial LRR proteins and to the plant defence protein PGIP. Structural comparison of the BRI1 ectodomain (shown as C_α trace in yellow; the island domain has been omitted for clarity) and the LRR domains of **a,** the extracellular bacterial effector protein YopM[31] (shown in blue, r.m.s.d. is 3.0 Å between 313 corresponding C_α atoms, DALI[61] Z-score is 20.0), **b,** the bacterial adhesion protein internalin A[32] (r.m.s.d. is 2.2 Å between 291 corresponding C_α atoms, DALI Z-score is 21.6), and **c,** the polygalacturonase-inhibiting protein (PGIP) from *Phaseolus vulgaris*[33] (r.m.s.d. is 2.3 Å between 252 corresponding C_α atoms, DALI Z-score is 19.8).

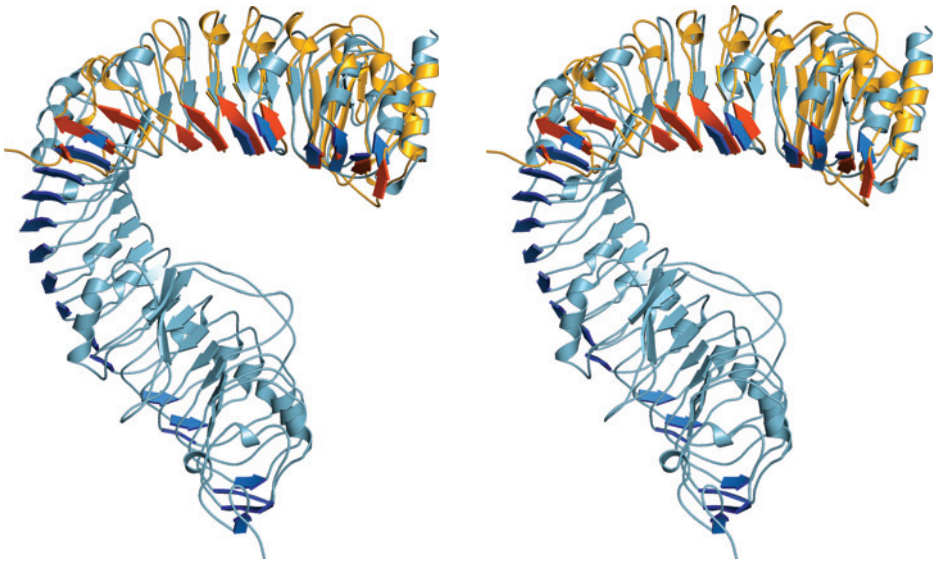

Supplementary Figure 3 | The plant LRR proteins PGIP and BRI1 contain additional β-sheets that cause supertwisting of their LRR domains. Stereo view of a structural superposition of the BRI1 ectodomain and the polygalacturonase-inhibiting protein (PGIP) from *Phaseolus vulgaris*[31] (r.m.s.d. is 2.3 Å between 252 corresponding C_α atoms). Both proteins are shown in ribbon representation, PGIP in yellow, BRI1 in light-blue. Note that the non-canonical β-sheet in PGIP (shown in dark-orange) that causes twisting of the PGIP LRR domain[33], is also present in BRI1 over the entire length of the molecule (shown in dark blue).

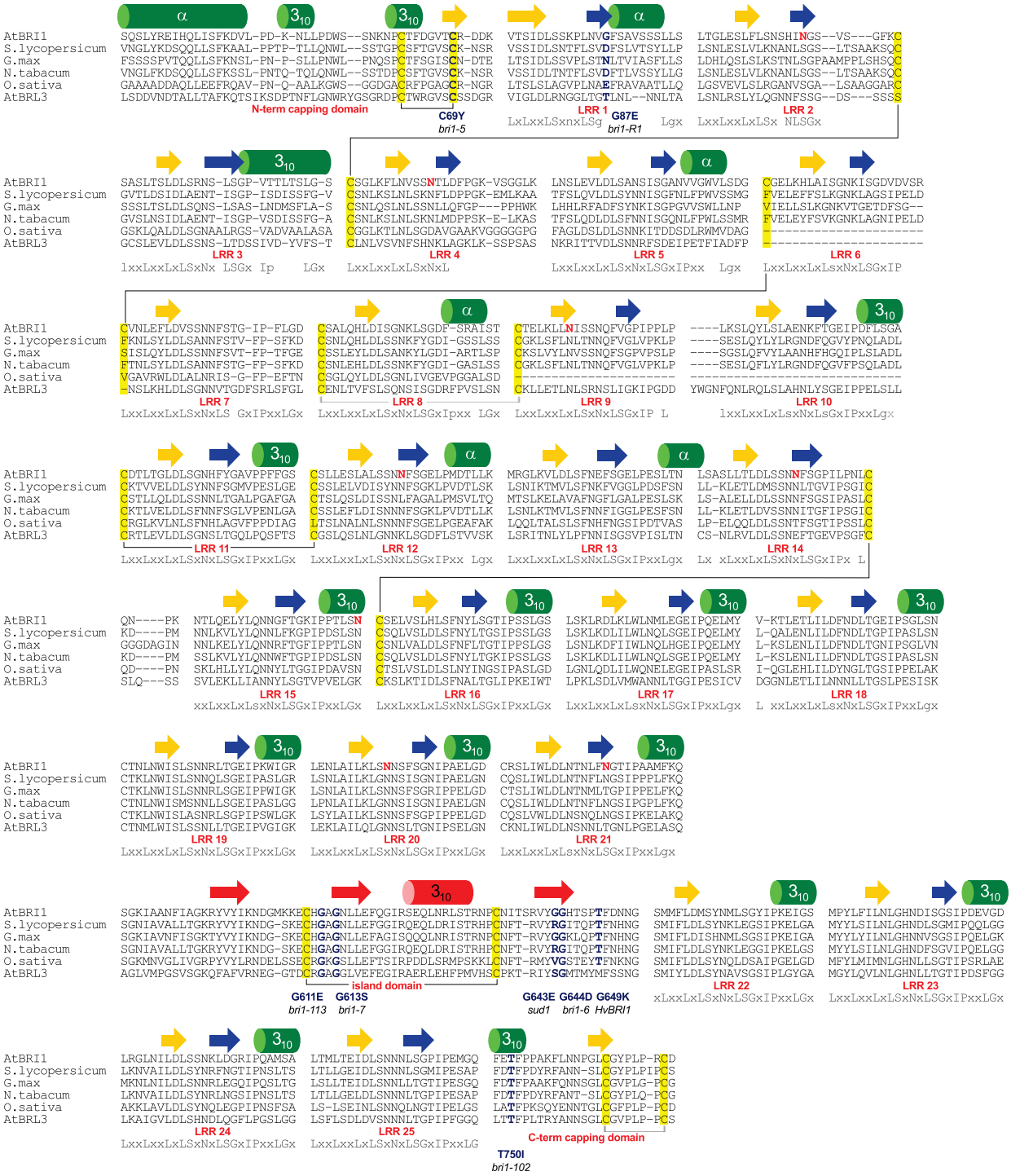

Supplementary Figure 4 | Key sequence fingerprints of the BRI1 ectodomain are conserved in BRI1 proteins from different plant species. Structure-based sequence alignment of representative BRI1 orthologs: *Arabidopsis thaliana* BRI1 UniProt (http://www.uniprot.org): O22476, residues 29-771), (*Solanum lycopersicum* (UniProt: Q8GUQ5, residues 37-780), *Glycine max* (UniProt: C6FF79, residues 21-765), *Nicotiana tabacum* (UniProt: A6N8J1, residues 46-787), *Oryza sativa* subsp. *japonica* (UniProt: Q942F3, residues 21-696), *Arabidopis thaliana* BRI1-like 3 (UniProt: Q9LJF3, residues 27-765). The alignment includes secondary structure assignments with DSSP[62], coloured according to Fig.1a. Cysteine residues in the LRRs and in the N- and C-terminal capping domains that form disulfide bonds are highlighted by yellow shading, N-glycosylation sites observed in the BRI1 structure are depicted with red letters. The positions of known missense alleles in the BRI1 ectodomain are indicated with blue lettering.

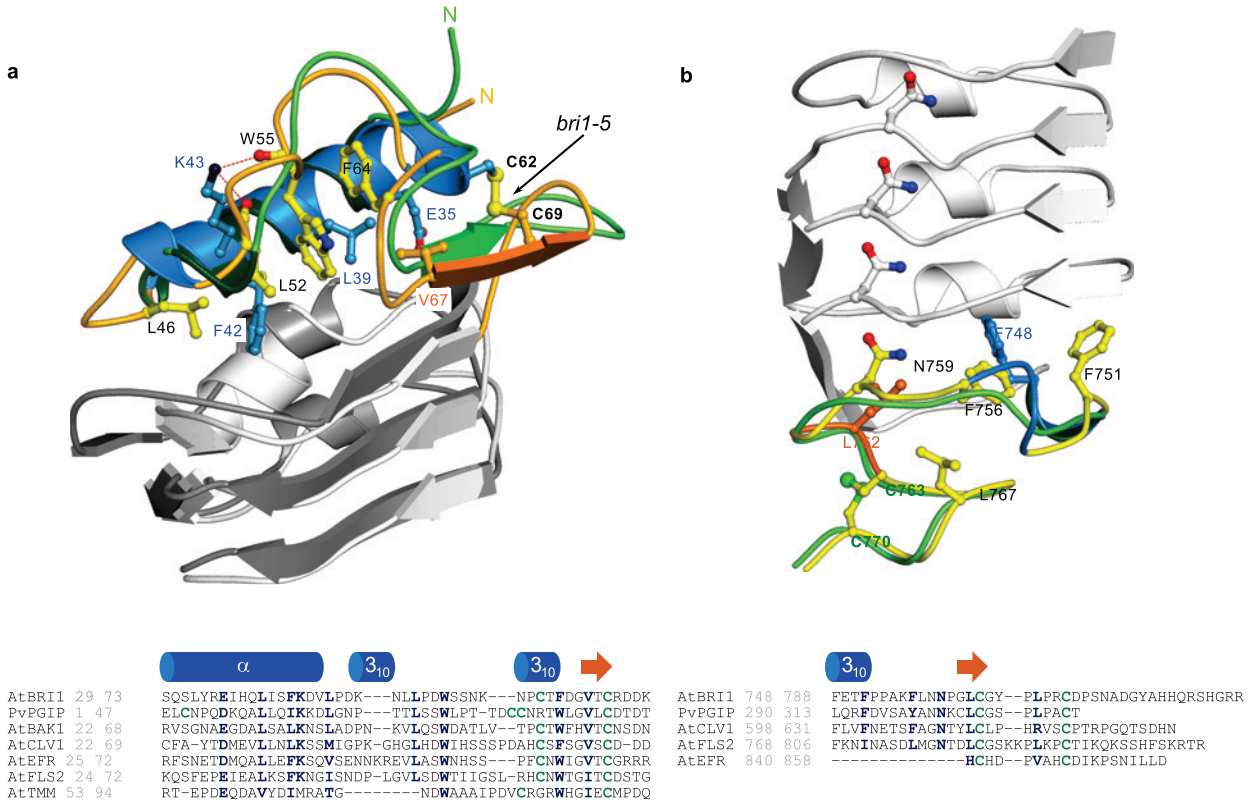

Supplementary Figure 5 | The BRI1 structure identifies plant-specific capping motifs. a, Ribbon diagram of the N-terminal capping structure, and **b,** of the C-terminal capping motif. The amphipatic α-helix and the small 3_{10} helices are shown in blue, and β-strands are depicted in orange. Conserved interfacing residues are highlighted in full atom representation. Mutation of Cys69 into Tyr (the genetic allele *bri1-5*) may destabilise the N-terminal cap in BRI1 and thus causes the receptor to be retained in the endoplasmic reticulum[35,63]. Superimposed in green are the corresponding caps from the plant defence protein PGIP that closely align with the BRI1 structure. Structure based sequence alignments that depict the corresponding capping motifs in the LRR-RKs BAK1[23,24],CLV1[4], EFR[7], FLS2[6] and TMM[5] suggest that similar capping structures are present in other plant receptor kinases.

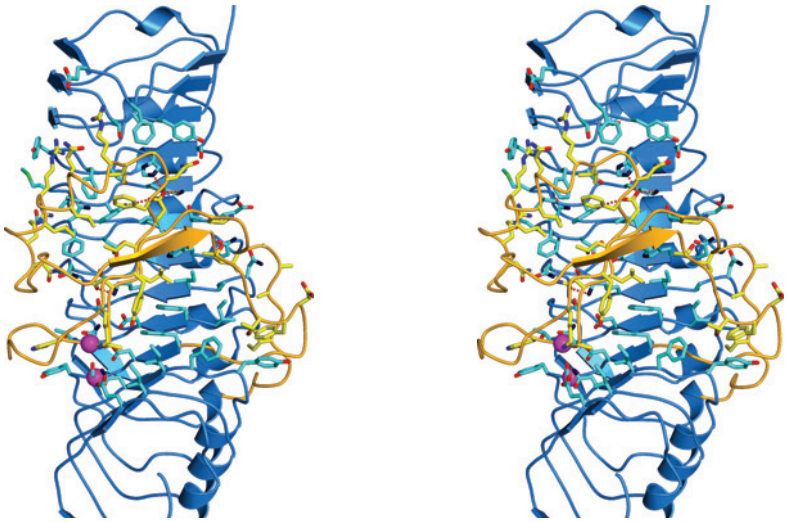

Supplementary Figure 6 | The island domain makes intensive contacts with the C-terminal LRR motifs in BRI1. Stereo view of LRRs 13-25 (ribbon diagram) in blue and the island domain (residues 584-654) in orange. Interface residues originating from the LRR core and the island domain are shown in light blue and yellow, respectively. Polar interactions (distance cut-off 3.5 Å) are depicted as dotted lines (in red). The BRI1 loss-of-function mutations Gly611Glu (*bri1-113*)[3] and Ser662Phe (*bri1-9*)[35] are highlighted by magenta balls.

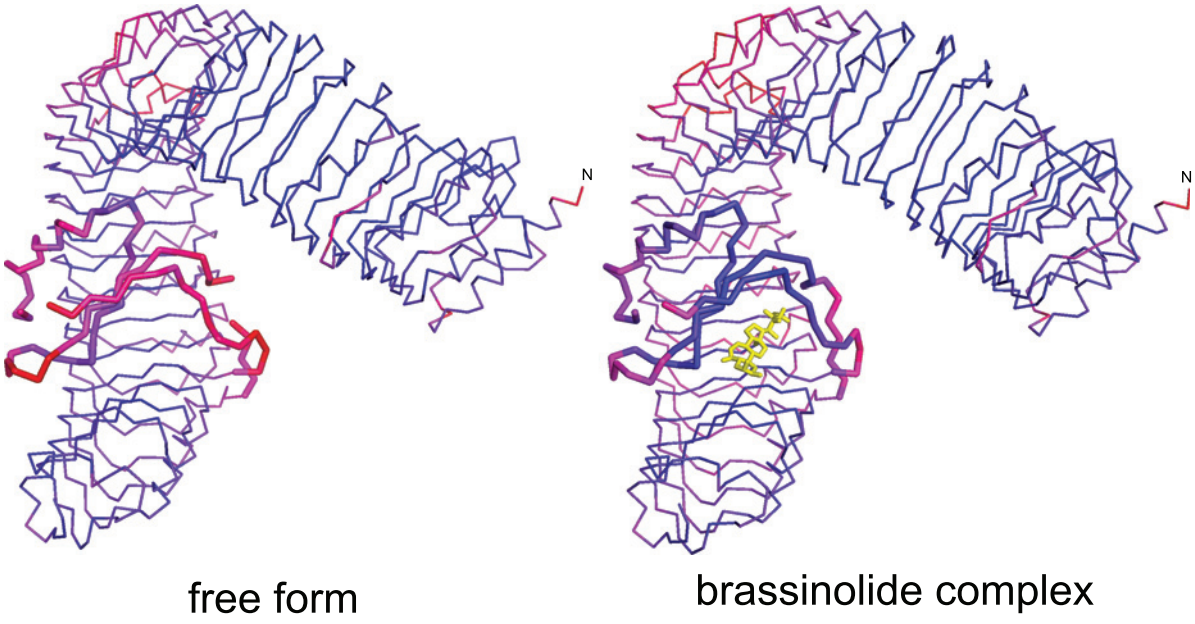

Supplementary Figure 7 | The island domain and the two connecting loops become fully ordered upon steroid hormone binding. Structural superposition of the free and brassinolide-bound ectodomain reveal no major conformational changes (r.m.s.d. <0.3 Å comparing 740 corresponding C_α atoms), but the entire island domain appears to be significantly better ordered in the steroid-complex when compared to the free structure. C_α trace views of the free and brassinolide bound structures coloured according to their crystallographic B-values (low (15 $Å^2$) to high (150 $Å^2$) corresponding to blue and red, respectively). The island domains are highlighted, and the steroid ligand is shown in sticks representation (in yellow). The average B-values for the LRR and island domains are 59.5 and 93.1 $Å^2$ (free from) and 64.4 and 65.5 $Å^2$ (brassinolide complex), respectively. Both the free and the steroid bound form crystallised under similar conditions, in the same space-group and with similar cell constants; and both diffracted to ~2.5 Å resolution (see Supplementary Methods).

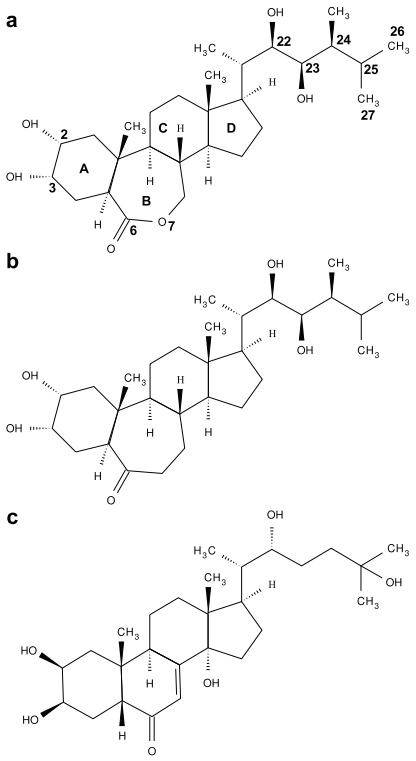

Supplementary Figure 8 | Chemical structures of different steroid ligands.
Chemical structures of the plant steroids **a,** brassinolide and **b,** castasterone and **c,** of the arthropod ecdysone. The ring nomenclature for brassinolide has been included in **a**.

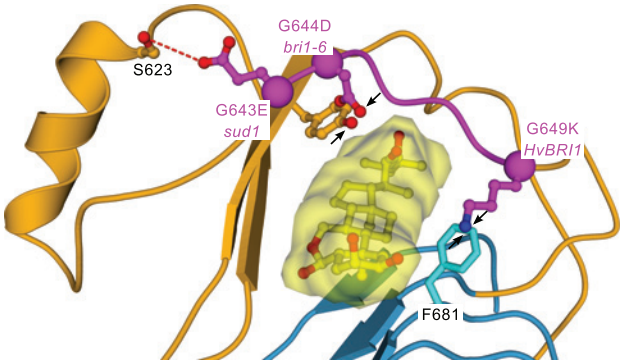

Supplementary Figure 9 | Genetic BRI1 missense alleles may affect the positioning of an island domain loop.
Close up view of the three genetic alleles that are located in a loop segment (residues 643 to 658) connecting the island domain with LRR 22. Gly643 that in the genetic allele *sud1* is mutated to Glu, may engage in a hydrogen bond with Ser623 in the island domain. This mutation may restrict movement of the loop segment and thus stabilise interaction with a co-receptor protein even in absence of steroid. Mutation of Gly644 into Asp causes the loss-of-function phenotype *bri1-6*, and mutation of the conserved Thr649 to Lys inactivates barley BRI1. These mutations seem to induce steric clashes with residues in the island domain and in the underlying LRR domain (indicated by black arrows) and may thus distort the overall position of the loop.

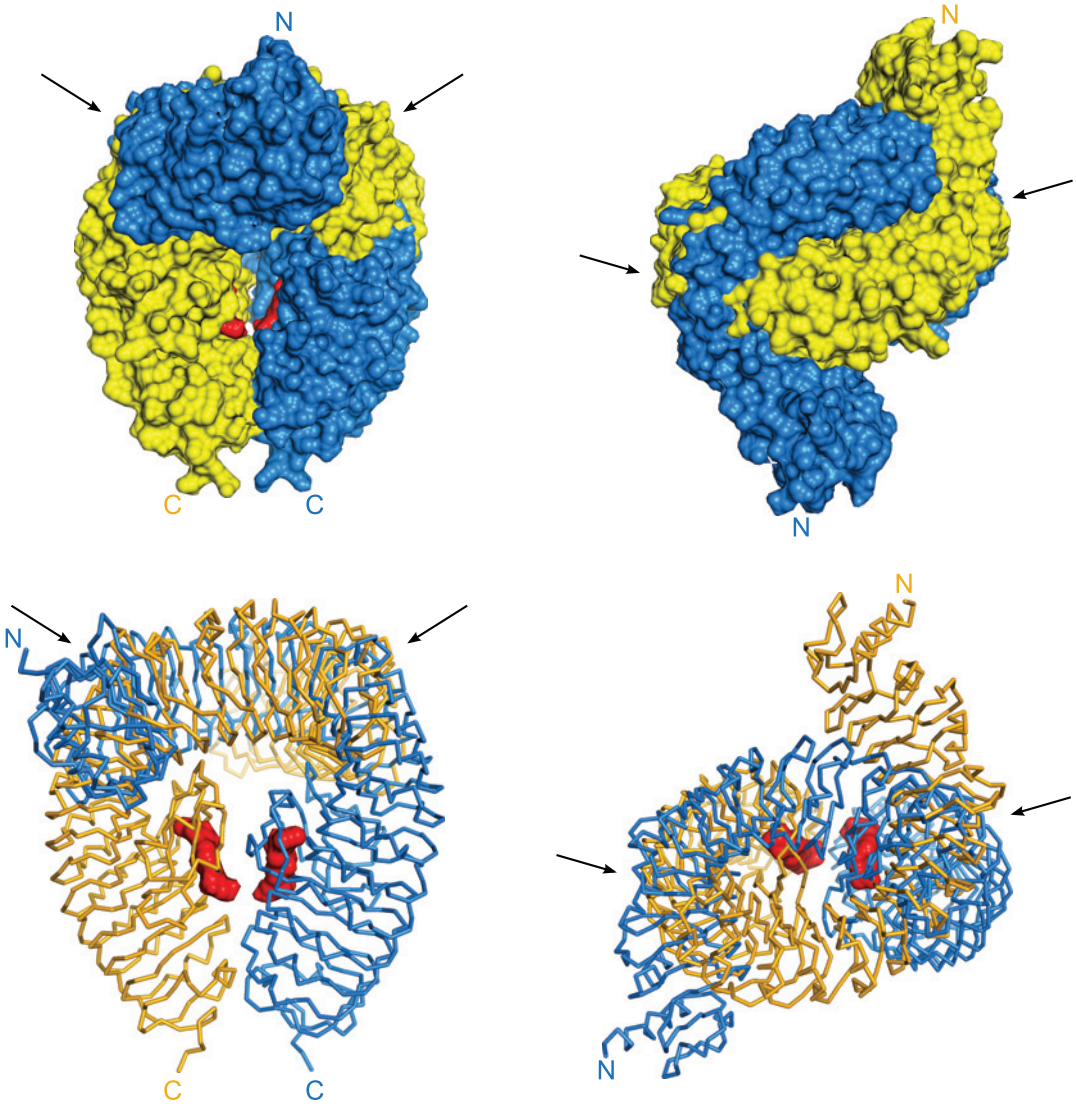

Supplementary Figure 10 | The superhelical BRI1 ectodomain is unlikely to dimerise. Hypothetical model of a BRI1 ectodomain homodimer in surface representations (top panel) and as a C_α trace (lower panel), with a front view on the left and a view from the top on the right. The model brings the C-termini of two neighbouring ectodomains (shown in blue, and yellow, respectively) in close proximity and employs the proposed protein interaction platform and the brassinosteroid ligand (in red) as the dimerisation interface. Note, that because of the superhelical shape of the ectodomain, this model causes severe clashes in the N-terminal LRRs of BRI1 (indicated by arrows).

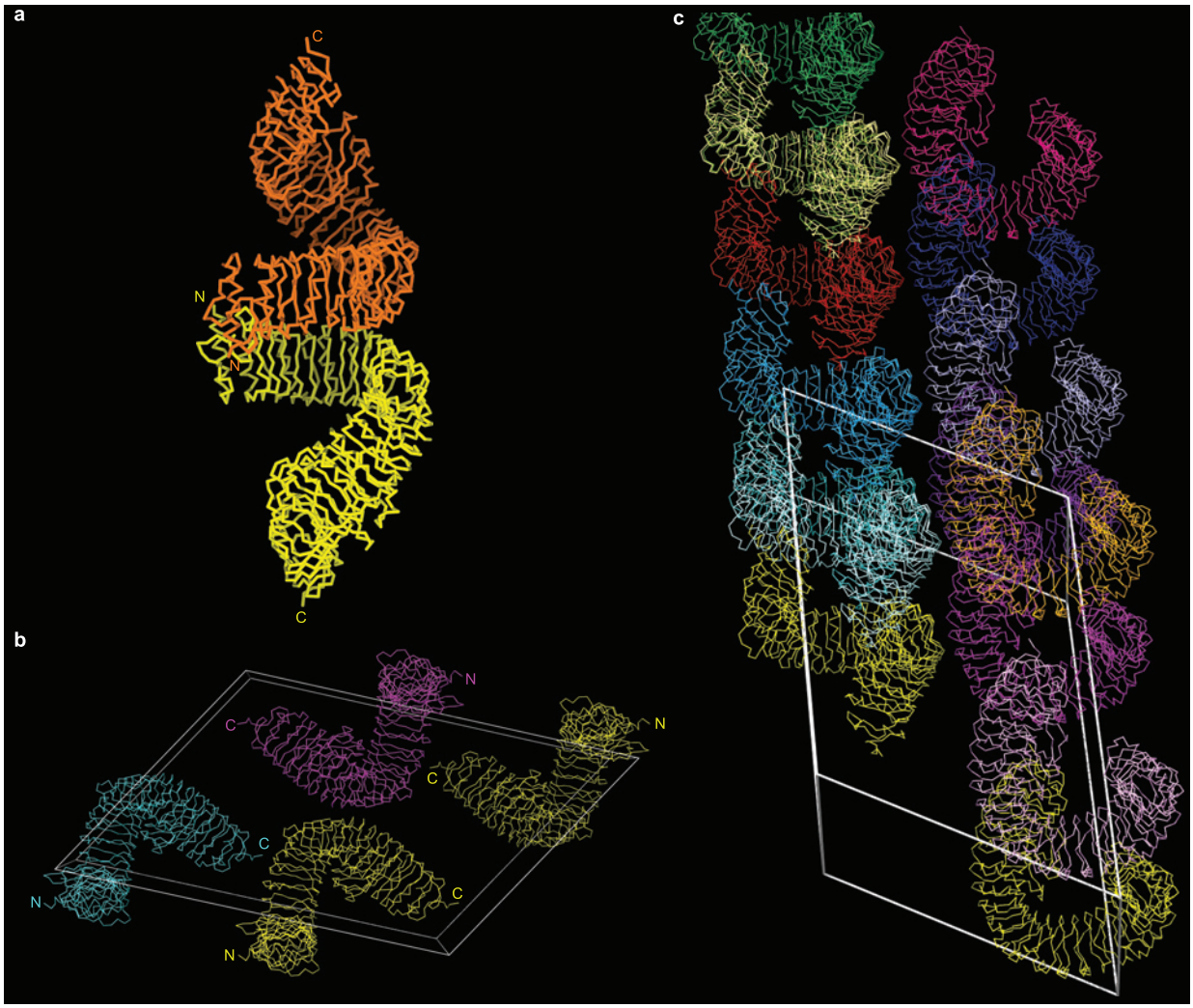

Supplementary Figure 11 | Crystal lattice packing analysis suggests the BRI1 ectodomain is monomeric. **a,** C_α trace of the major lattice contact observed in the monoclinic BRI1 crystals. The interface brings two neighbouring molecules in a head-to-head configuration with their C-termini far apart at opposite ends. **b,** View of the second minor crystal contact that involves interaction of two BRI1 molecules with their outer helix surfaces along the 2-fold symmetry axis. **c,** Crystal packing of BRI1 molecules along a. The BRI1 superhelix propagates itself using the head-to-head contacts described in **a**.

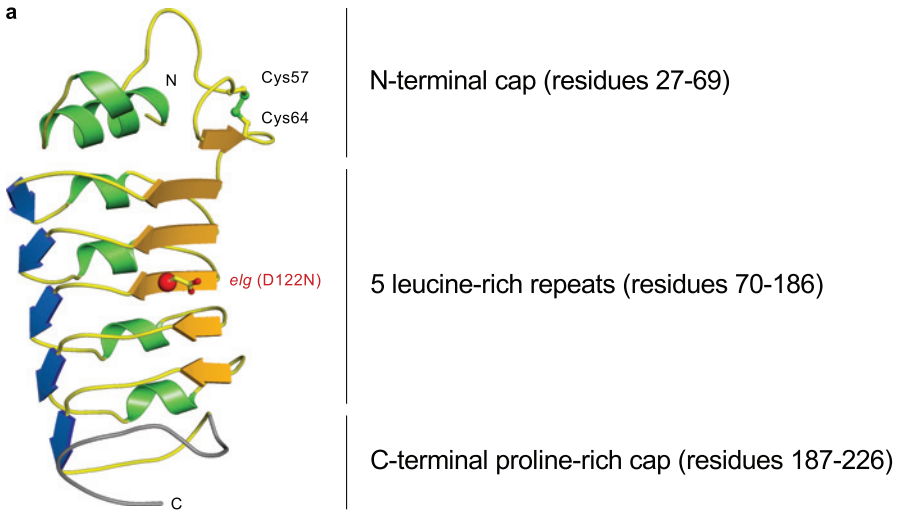

b

		1	2	3	4	5	6	7	8	9	10	11	12	13	14	15	16	17	18	19	20	21	22	23	24	
LRR	*beg*	L	X	X	L	X	X	L	X	L	S	X	N	X	L	S	G	X	I	P	X	X	L	G	X	*end*
1	*70*				V	T	R	V	D	L	G	N	A	N	L	S	G	Q	L	V	M	Q	L	G	Q	*90*
2	*91*	L	P	N	L	Q	Y	L	E	L	Y	S	N	N	I	T	G	T	I	P	E	Q	L	G	N	*114*
3	*115*	L	T	E	L	V	S	L	D	L	Y	L	N	N	L	S	G	P	I	P	S	T	L	G	R	*138*
4	*139*	L	K	K	L	R	F	L	R	L	N	N	N	S	L	S	G	E	I	P	R	S	L	T	A	*162*
5	*163*	V	L	T	L	Q	V	L	D	L	S	N	N	P	L	T	G	D	I	P	V	N	G	S	F	*186*

Supplementary Figure 12 | Homology model of the BAK1 ectodomain a, Ribbon diagram of a homology model of the BAK1 ectodomain based on the crystal structures of BRI1 (this study) and PGIP[33] generated with the program MODELLER[59] (see Supplementary Methods). Our model suggests that the N-terminal residues 27-69 do not form a leucine zipper motif as previously suggested[23], but an N-terminal capping motif that is highly similar to that in BRI1 and PGIP (see Supplementary Fig. 5). In agreement with earlier predictions[23,24], our BAK1 model contains 5 repeats that contain the canonical β-strand (in orange), followed by the non-canonical β-strand found in the plant-specific LRR subfamily[34] (in blue), and a 3_{10} helix (in green). The BAK1 *elg* allele[46], which renders mutant plants hypersensitive to brassinosteroid treatment[47], maps to the inner surface of the BAK1 ectodomain. The C-terminal capping motif is a proline-rich motif that in sequence deviates from the C-terminal capping motifs found in BRI1 and PGIP (see Supplementary Fig. 5), and therefore could not be modelled with confidence (in grey). **b,** The family-defining sequence fingerprints of the plant-specific LRR subfamily (Lt/sGxIP)[34] are present in all 5 LRR repeats in BAK1 (in green). The position of the *elg* mutation is indicated in red.

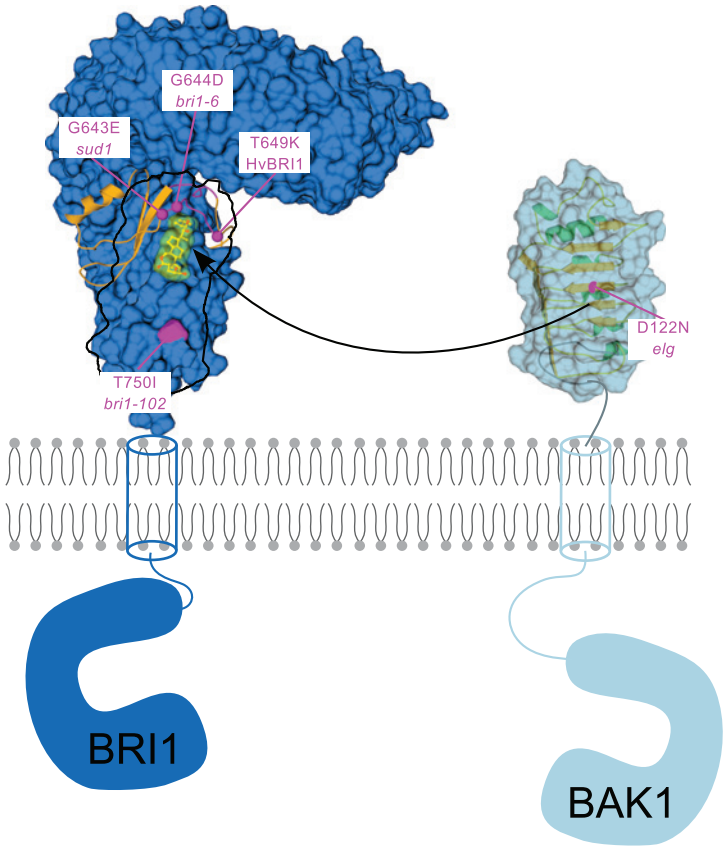

Supplementary Figure 13 | Speculative model for BRI1 receptor activation by heteromerisation with the smaller co-receptor kinase BAK1. Side-by-side view of the BRI1 ectodomain structure (surface representation, in dark-blue) and the BAK1 homology model (in light-blue) suggests that the BAK1 ectodomain is compatible in size and shape with the protein interaction surface in BRI1. We hypothesise that steroid binding to BRI1 generates a docking platform for the ectodomain of BAK1. We envision this docking platform in BRI1 to be composed of the steroid ligand itself, of parts of the island domain (in orange) (especially the connecting loops that become ordered upon steroid binding, in magenta), and of surface patches of the LRR domain (i.e. Thr750, whose mutation to isoleucine causes the loss-of-function phenotype *bri1-102*[41], in magenta). Steroid-dependent heteromerisation of the BRI1 and BAK1 ectodomains would bring their cytoplasmic juxtamembrane regions and kinase domains in close proximity, where they could transphosphorylate each other, leading to receptor activation and phosphorylation of downstream signalling partners. This mechanism would still be plausible if BRI1 molecules form constitutive homooligomers at plant membranes, as long as the interaction surfaces for BAK1 are still accessible in these oligomers. We envision that the gain-of-function alleles *sud1*[39] in BRI1 and *elg*[46,47] in BAK1 stabilise formation of the heteromeric complex, and that loss-of-function alleles *bri1-6*[35], *bri1-102*[41] and the mutation in barley BRI1[40] (Thr649 in AtBRI1) (all in magenta) destabilise interaction of the BAK1 and BRI1 ectodomains.

Supplementary Table 1 | Data collection and refinement statistics.

	unbound (NaI soak)	unbound (native)	brassinolide-complex
Data collection			
Space group	*C*2	*C*2	*C*2
Cell dimensions			
a, b, c (Å)	175.04, 67.53, 119.83	175.09, 67.25, 119.05	175.11, 67.21, 119.21
β angle (°)	121.06	121.55	121.41
Wavelength (Å)	1.5418	0.9998	1.5418
Resolution (Å)	29.28 – 2.90	31.00-2.52	24.64 – 2.54
Highest shell (Å)	2.97 – 2.90	2.68 – 2.52	2.69 – 2.54
No. unique reflections*	26,445 (1,625)	39,686 (6,145)	38,900 (5,904)
R_{sym} (%) †	8.0 (47.8)	5.5 (58.3)	6.0 (48.2)
$I/\sigma I$	22.2 (4.1)	17.6 (2.1)	14.9 (2.3)
Completeness (%)	97.7 (81.4)	98.8 (95.3)	98.6 (93.8)
Multiplicity	14.2 (10.5)	3.7 (3.5)	4.1 (3.5)
Refinement			
Resolution (Å)		31.00 – 2.52	24.64 – 2.54
Highest shell (Å)		2.61-2.52	2.63 – 2.54
No. reflections		39,686 (3,575)	38,849 (3,537)
R_{work}‡		0.185 (0.321)	0.184 (0.263)
R_{free}‡		0.236 (0.409)	0.240 (0.332)
No. atoms			
Protein/glycan		5,544 / 170	5,558 / 192
Water/brassinolide		129	114 / 34
B-factors (Å^2)			
Wilson B		55.0	51.8
Protein/glycan		62.5 / 92.9	64.5 / 89.3
Water/brassinolide		53.0	51.4 / 47.8
R.m.s. deviations			
bond length (Å)		0.006	0.006
bond angles (°)		1.02	1.05

* Numbers in parentheses provide statistics for the highest resolution shell
† As defined in XDS[51]
‡ As defined in phenix.refine[56]

		1	2	3	4	5	6	7	8	9	10	11	12	13	14	15	16	17	18	19	20	21	22	23	24		No.		
LRR	*beg*	**L**	**X**	**X**	**L**	**X**	**X**	**L**	**X**	**L**	**S**	**X**	**N**	**X**	**L**	**S**	**G**	**X**	**I**	**P**	**X**	**X**	**L**	**G**	**X**	*end*	**res**	**β2**	**isl./lig.**
1	*74*				V	T	S	I	D	L	S	S	K	P	L	N	V	G	F	S	A	V	S	SL	LS	*97*	23	+	/
2	*98*	L	T	G	L	E	S	L	F	L	S	N	S	H	I	N	G	S	V	S	G	F	K	***C***		*120*	23	+	/
3	*123*	S	A	S	L	T	S	L	D	L	C	R	N	S	L	S	G	P	V	T	T	L	T	SL	GS	*146*	26	+	/
4	*147*	***C***	S	G	L	K	F	L	N	V	S	S	N	T	L	D	F	P	G	K	V	S	G	G	LK	*171*	25	+	/
5	*172*	L	N	S	L	E	V	L	D	L	S	A	N	S	I	S	G	A	N	V	V	G	WV	LS	DG	*198*	27	+	/
6	*199*	***C***	G	E	L	K	H	L	A	I	S	G	N	K	I	S	G	D					V	S	R	*220*	20	+	/
7	*221*	***C***	V	N	L	E	F	L	E	V	S	S	N	N	F	S	T	G	I	P	F		L	G	D	*243*	23		/
8	*244*	***C***	S	A	L	Q	H	L	D	I	S	G	N	K	L	S	G	D	F	S	R	A	I	S	T	*267*	24		/
9	*268*	***C***	T	E	L	K	L	L	N	I	S	S	N	Q	F	V	G	P	I	P	P		L	P		*289*	22	+	/
10	*290*	L	K	S	L	Q	Y	L	S	L	A	E	N	K	F	T	G	E	I	P	D	F	L	SG	A	*314*	25	+	/
11	*315*	***C***	D	T	L	T	G	L	D	L	S	G	N	H	F	Y	G	A	V	P	P	F	F	G	S	*338*	24	+	/
12	*339*	***C***	S	L	L	E	S	L	A	L	S	S	N	N	F	S	G	E	L	P	M	DT	L	L	K	*363*	25	+	/
13	*364*	M	R	G	L	K	V	L	D	L	S	**F**	N	**E**	F	S	G	E	L	P	E	S	L	T	N	*387*	24	+	+/
14	*388*	L	S	AS	L	L	T	L	D	L	S	**S**	N	**N**	F	S	G	P	I	L	P	N	L	***C***		*411*	24	+	+/
15	*416*		N	T	L	Q	E	L	**Y**	L	**Q**	**N**	N	**G**	F	T	G	K	I	P	P	T	L	S	N	*438*	23	+	+/
16	*439*	***C***	S	E	L	V	**S**	L	**H**	L	**S**	**F**	N	**Y**	L	S	G	T	I	P	S	SS	L	G	S	*462*	25	+	+/
17	*463*	L	S	K	L	R	D	L	**K**	L	**W**	**L**	N	**M**	L	E	G	E	I	P	Q	E	L	M	Y	*486*	24	+	+/
18	*487*	V	K	T	L	**E**	**T**	L	**I**	L	**D**	**F**	N	**E**	L	T	G	E	I	P	S	G	L	S	N	*510*	24	+	+/
19	*511*	**C**	T	N	L	**N**	**W**	I	**S**	L	**S**	**N**	N	R	L	T	G	E	I	P	K	W	I	G	R	*534*	24	+	+/
20	*535*	L	E	N	L	**A**	**I**	L	**K**	L	**S**	N	N	S	F	S	G	N	I	P	A	E	L	G	D	*558*	24	+	+/
21	*559*	**C**	R	S	L	**I**	**W**	L	**D**	L	N	**T**	**N**	L	F	N	G	T	I	P	A	A	MF	K	Q	*583*	25	+	+/+
22	*655*			S	M	M	F	L	D	M	S	Y	N	M	L	S	G	Y	I	P	K	E	I	G	S	*676*	22		+/+
23	*677*	M	P	**Y**	L	**F**	**I**	L	**N**	L	G	H	N	D	I	S	G	S	I	P	D	E	V	G	D	*700*	24	+	+/+
24	*701*	L	R	G	L	N	**I**	L	D	L	S	S	N	K	L	D	G	R	I	P	Q	A	M	S	A	*724*	24	+	+/+
25	*725*	L	T	M	L	T	**E**	I	D	L	S	N	N	N	L	S	G	R	I	P	Q	A	M	G	Q	*747*	24	+	+/+

Supplementary Table 2 | Sequence fingerprints of the LRR domain in BRI1. The BRI1 repeat sequences are arranged according to a canonical 24 residue LRR motif of the plant-specific family of LRR proteins. The beginning and end of each LRR, its total length, the presence of the non-canonical β-strand (β2) are shown. Involvement of the respective LRR in formation of an interface with the island domain (isl.) or in steroid hormone binding (lig.) is indicated. Residues that are part of the LRR-island domain interface are highlighted in blue, the Cys residues in position and 1 and 24 are shown in green. Cysteines in italics are engaged in disulfide bridges.